


## Docetaxel prodrug and hematoporphyrin co-assembled nanoparticles for anti-tumor combination of chemotherapy and photodynamic therapy

Guolian Ren<sup>a,†</sup> , Yujie Li<sup>a,†</sup>, Canqi Ping<sup>a</sup>, Danyu Duan<sup>a</sup>, Ning Li<sup>a</sup>, Jiaqi Tang<sup>a</sup>, Rongrong Wang<sup>a</sup>, Wenju Guo<sup>a,b</sup>, Xiaomin Niu<sup>a</sup>, Qiuyue Ji<sup>a</sup>, Guoshun Zhang<sup>a</sup>, Ruili Wang<sup>a</sup> and Shuqiu Zhang<sup>a</sup>

<sup>a</sup>School of Pharmacy, Shanxi Medical University, Taiyuan, China; <sup>b</sup>Department of Pharmacy, Shanxi Bethune Hospital, Taiyuan, China

### ABSTRACT

To realize the synergistic anti-tumor effect of chemotherapy and photodynamic therapy, the mono sulfide-modified docetaxel (DTX) prodrugs (DSD) provided by our laboratory and hematoporphyrin (HP) were used to physically prepare co-assembled nanoparticles (DSD/HP NPs) by nano-precipitation. For the first time, this study showed its characteristics, *in vitro* anti-tumor activity, pharmacokinetic behavior in rats, *in vivo* distribution, and pharmacodynamic effects on 4T1 tumor-bearing Bal b/c mice. DSD/HP NPs optimized by single-factor and response surface optimization had several distinct characteristics. First, it had dark purple appearance with particle size of  $105.16 \pm 1.24$  nm, PDI of  $0.168 \pm 0.15$ , entrapment efficiency and drug loading of DSD and HP in DSD/HP NPs of  $96.27 \pm 1.03\%$  and  $97.70 \pm 0.20\%$ ,  $69.22 \pm 1.03\%$  and  $20.03 \pm 3.12\%$ , respectively. Second, it had good stability and could release DTX and HP slowly in the media of pH 7.4 PBS with 10 mM DTT ( $H_2O_2$ ). Moreover, DSD/HP NPs along with NiR treatment significantly inhibited 4T1 cells proliferation, and induced more reactive oxygen species and cells apoptosis. *In vivo* pharmacokinetic and pharmacodynamic studies showed that DSD/HP NPs could prolong the drug circulation time in rats, increase drug distribution in tumor site, obviously inhibit tumor growth, and decrease the exposure of drug to normal tissues. Therefore, DSD/HP NPs as a promising co-assembled nano-drug delivery system could potentially improve the therapeutic efficiency of chemotherapeutic drug and achieve better anti-tumor effects due to the combination of chemotherapy and photodynamic therapy.

### ARTICLE HISTORY

Received 10 October 2022  
Revised 7 November 2022  
Accepted 7 November 2022

### KEYWORDS

Docetaxel prodrug;  
hematoporphyrin;  
co-assembled nanoparticles;  
chemotherapy; photodynamic  
therapy

## 1. Introduction

Breast cancer is the second most common cancer in the world after lung cancer (Lisa, 2010; Tohkayomatee et al., 2022). Its morbidity and mortality are increasing year by year to threaten the health of women (Chaffer & Weinberg, 2011; Koual et al., 2020; Rabiei et al., 2022). Chemotherapy is one of the main ways to treat breast cancer. Docetaxel (DTX) acted as a commonly used first-line chemotherapy drug for breast cancer has poor solubility and weak membrane permeability (Gong et al., 2020; Razak et al., 2021). However, the commercial preparation of Taxotere<sup>®</sup> has some side effects such as acute hypersensitivity and hemolysis, which attribute to the application of tween 80 and ethanol in preparation (Gong et al., 2020). As a result, its application in clinic is restrict. To alleviate these problems, improve efficacy, and develop DTX preparations with better therapeutic effects, recent studies on the strategy of prodrug loaded nano-drug delivery system were carried out to find the least risky and


best treatment (Li et al., 2021; Peng et al., 2021; Ren et al., 2022).

At present, the prodrug loaded self-assembled nanoparticles acted as a unique nano-drug delivery strategy has some advantages such as high drug loading (DL), good stability, selective drug release, and improved anti-tumor effects (Ren et al., 2016; Yang et al., 2020; Li et al., 2021; Ren et al., 2022). Therefore, according to the physical and chemical properties of DTX, appropriate DTX prodrugs were synthesized and prepared to be an effective self-assembled nanoparticles to improve its therapeutic effects (Wohl et al., 2014).

In our previous study, n-dodecanol (Do)-modified DTX prodrug with mono sulfide bond as linker (DSD) was successfully synthesized, and prepared as nanostructure lipid carrier (DNLC) (Tang et al., 2020). The results of *in vitro* release found that the release of DTX from DNLC was redox sensitivity, and *in vivo* pharmacokinetic and pharmacodynamic study showed that DNLC significantly increased the concentration of DTX in plasma after intravenous administration to

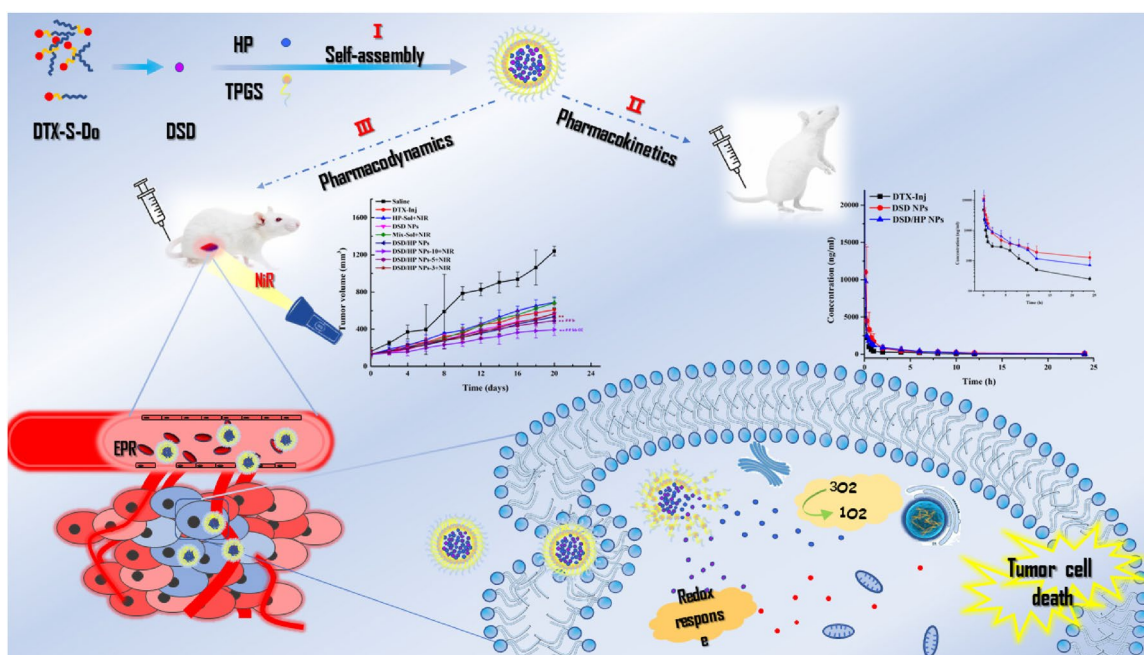
**CONTACT** Guolian Ren  [gren2007@126.com](mailto:gren2007@126.com); Shuqiu Zhang  [shuqiu.zhang@126.com](mailto:shuqiu.zhang@126.com)  School of Pharmacy, Shanxi Medical University, 56 Xinjian South Road, Taiyuan 030001, China

<sup>†</sup>These authors contributed equally to this work.

 Supplemental data for this article can be accessed online at <https://doi.org/10.1080/10717544.2022.2147280>

© 2022 The Author(s). Published by Informa UK Limited, trading as Taylor & Francis Group.

This is an Open Access article distributed under the terms of the Creative Commons Attribution-NonCommercial License (<http://creativecommons.org/licenses/by-nc/4.0/>), which permits unrestricted non-commercial use, distribution, and reproduction in any medium, provided the original work is properly cited.



**Scheme 1.** Schematic illustration of DSD/HP co-assembled nano-drug delivery system for the combination of nanotechnology, chemotherapy, and photodynamic therapy. I DSD and HP were successfully prepared to be as co-assembled nanoparticles (DSD/HP NPs) using the method of nanoprecipitation. II DSD/HP NPs were administered to rats intravenously to prolong the drugs circulated time in blood. III The designed DSD/HP NPs improved the accumulation of drugs in tumor site, produced more ROS to induce 4T1 cells apoptosis, and initiated the antitumor efficiency of chemotherapy and locoregional photodynamic therapy.

rats, and had good anti-tumor efficacy and low toxicity. So, in this study, DSD used as a model drug combined with hematoporphyrin (HP) to prepare co-loaded self-assembled nanoparticles (DSD/HP NPs) for further study on their anti-tumor effects. Here, HP is widely selected as a photosensitizer used in photodynamic therapy (PDT), which is a non-surgical and innovative method with low systematic toxicity, minimally invasive, and high selectivity to tumor tissue for the treatment of small and superficial tumors (Chang et al., 2014; Abrahamse & Hamblin, 2016; Allison & Ferguson, 2022; Li et al., 2022; Wang et al., 2022). PDT as a new type of tumor treatment has three key factors of light, photosensitizer (PS), and reactive oxygen species (ROS) (Agostinis et al., 2011; Abrahamse & Hamblin, 2016; Plekhova et al., 2022). Under the irradiation of near infrared ray (NiR) at a specific excitation wavelength, PS is activated to produce a photochemical reaction, which then induces the production of ROS to directly kill cancer cells (Dąbrowski & Arnaut, 2015; Menilli et al., 2022; Xue et al., 2022). Meanwhile, ROS can also destroy tumor vasculature, activate the host's anti-tumor immune response, indirectly play anti-tumor effect (Dąbrowski & Arnaut, 2015; Fan et al., 2017; Menilli et al., 2022). Thus, PDT has attracted great attention from researchers as a non-invasive and highly selective approach for cancer treatment, and HP has high phototoxicity and can be rapidly metabolized from human tissues (Castano et al., 2005; Abrahamse & Hamblin 2016; Kim et al., 2020; Zhu et al., 2022). However, there are still certain defects of HP. For example, HP is a hydrophobic drug with low water solubility, so it is not easy to make an intravenous injection directly (Wu et al., 2022).

In this article, to elevate the anti-tumor effects of DSD with HP, co-loaded self-assembled nano-precipitation technology was employed to combine DSD with HP as DSD/HP NPs, which

were prepared to further expand research depth and achieve a synergistic effect of the combinative treatment of chemotherapy and PDT (Fan et al., 2014; Zhu et al., 2021, 2022). The optimization, stability, *in vitro* release, *in vitro* cytological evaluation, *in vivo* pharmacokinetics, and pharmacodynamics of DSD/HP NPs with or without the treatment of NiR were investigated to evaluate the anti-tumor effects (Scheme 1).

## 2. Materials and methods

### 2.1. Materials

DTX and paclitaxel (PTX) were purchased from Nanjing Jingzhu Biotechnology Co., Ltd (Nanjing, China). DTX prodrug (DTX-S-Do, DSD) was provided by our laboratory. HP was purchased from Med Chem Express. 4-dimethylaminopyridine (DMAP), N-(3-Dimethylaminopropyl)-N'-ethylcarbodiimide hydrochloride (EDCI), and Vitamin E polyethylene glycol succinate (TPGS) were obtained from Aladdin Biotechnology Co., Ltd (Shanghai, China). Cell Counting Kit-8 (CCK-8) was purchased from Sigma-Aldrich Inc (MO, USA). ROS Detection Assay Kit was purchased from Elabscience Biotechnology Co., Ltd (Wuhan, China). DTX injection (DTX Inj) was purchased from Jiangsu Aosaikang Pharmaceutical Co., Ltd. All other reagents were analytical level.

### 2.2. Animals

Female Sprague-Dawley rats (6-8 weeks old, weighing 180-220g) and female Bal b/c mice (6-8 weeks old, weighing 18-22g) were selected to use in this study. All the animals were provided by the Animal Center of Shanxi Medical University (Shanxi, China).

### 2.3. Preparation of docetaxel prodrug/hematoporphyrin co-assembled nanoparticles

DSD/HP NPs were prepared by our prescribed method (Li et al., 2020). DSD, HP, and TPGS at a certain amount were dissolved with 1 mL anhydrous ethanol solution. Then it was injected slowly into suitable distilled water at a certain stirring speed. After removing the solvent of ethanol by rotary evaporator, DSD/HP NPs were obtained and stored at 4°C.

### 2.4. Optimization of docetaxel prodrug/hematoporphyrin co-assembled nanoparticles

Response surface method (RSM) was used to optimize the prescription of DSD/HP NPs. The molar ratio of HP to DSD, content of DSD, and stabilizer were selected as influencing factors. The particle size, PDI, EE of DSD, and EE of HP were used as response values of response surface experiments. The desirability function of particle size and PDI was at the minimum level, and that of EE was at the maximum level to optimize the prescription. According to the Box-Behnken test design (BBD), the experimental conditions were designed and optimized.

### 2.5. Characterization of docetaxel prodrug/hematoporphyrin co-assembled nanoparticles

The particle size, PDI, and zeta potential of DSD/HP NPs were measured using a Malvern Zetasizer Nano ZS (Malvern, UK). The morphology of DSD/HP NPs was observed by transmission electron microscopy (TEM, JEM-2010, Japan).

DL and EE of DSD and HP in DSD/HP NPs were measured by centrifugalization. Briefly, 1 mL DSD/HP NPs was placed in 1.5 mL EP tube. Then it was centrifuged at 3500 r/min for 20 min. 500  $\mu$ L supernatant after centrifugalization and suspensions before centrifugalization were put into 5 mL volumetric flask, and dissolved with acetonitrile solution and anhydrous ethanol solution, respectively. After that they were vortexed 5 min and continued to ultrasonic for 5 min. DL and EE were calculated according the following equations.

$$EE = \frac{W_1}{W_2} \times 100\%$$

$$DL = \frac{W_1}{W_3} \times 100\%$$

$W_1$  was amounts of drugs loaded into DSD/HP NPs.  $W_2$  was total amounts of drugs added, and  $W_3$  was total amounts of the substances used to prepare DSD/HP NPs.

### 2.6. The stability of docetaxel prodrug/hematoporphyrin co-assembled nanoparticles

The stability of DSD/HP NPs was studied under ten times dilution, which was diluted with water, saline, phosphate buffer saline (PBS, pH7.4), and RPMI-1640 medium. Then the samples were placed in a thermostatic water bath oscillator with a stirring speed of 100 r/min at  $37 \pm 2^\circ\text{C}$  for 36 h.

Meanwhile, another batch of samples was stored at 4°C for 30 d, respectively. At the designed time, the particle size and PDI of samples were measured to evaluated the physical and long-term stability, respectively.

### 2.7. The release kinetics analysis of docetaxel prodrug/hematoporphyrin co-assembled nanoparticles

The small cup method was used to evaluate *in vitro* release behavior of DTX in DSD/HP NPs. Briefly, 2 mL of DSD/HP NPs with DSD concentration of 2.0 mg/mL was dispersed in 10 mL PBS solution containing 30% ethanol with or without 10 mM  $\text{H}_2\text{O}_2$  and DTT. Then, it was placed in a shaker at the speed of 100 r/min under the temperature of  $37.0 \pm 0.5^\circ\text{C}$ . At the predesigned time, 1 mL of sample solution was taken out and centrifuged at 3500 r/min for 20 min. Then, the precipitate was dissolved with 1 mL acetonitrile and vortexed for 1 min. Subsequently, it was transferred to a 5 mL volumetric flask and diluted with acetonitrile to volume, which was ultrasonic for 10 min. The content of DSD was analyzed by HPLC on a C18 column at the mobile phase of acetonitrile/water (90:10, v/v) under a flow rate of 0.8 mL/min. And the detection wavelength was set at 230 nm. Meanwhile, the content of HP released from DSD/HP NPs was also evaluated using a Thermo Scientific Microplate Reader with an excitation of 405 nm and emission of 598 nm. The drug release kinetics was analyzed on zero order, first order, and Higuchi models.

### 2.8. Cell culture

4T1 cells was a mouse metastatic breast cancer cell line. 4T1 cells frozen in liquid nitrogen container were quickly thawed in  $37^\circ\text{C}$  water bath within 1 min. Then, it was transferred into a centrifuge tube under a clean bench. And 4T1 cells were cultured in RPMI 1640 containing 10% FBS, 100  $\mu\text{g}/\text{mL}$  penicillin, and 100  $\mu\text{g}/\text{mL}$  streptomycin in a humidified atmosphere containing 5%  $\text{CO}_2$  at  $37^\circ\text{C}$ .

### 2.9. Cytotoxicity analysis

The cytotoxicity of DSD/HP NPs combined with or without PDT was investigated in 4T1 cells by CCK-8 assay. Briefly, 100  $\mu\text{L}$  of 4T1 cells ( $3 \times 10^4$  cells/mL) were planted into each well of 96-well plate. After 24 h incubation, the cells were treated with DTX-Sol, DSD NPs, MIX-Sol, DSD/HP NPs, MIX-Sol+NiR, and DSD/HP NPs+NiR diluted with serum-free cell culture medium for 4 h. Then, the cells treated with MIX-Sol+NiR and DSD/HP NPs+NiR were additionally irradiated with a PDT laser (630 nm, 100 mW/cm<sup>2</sup>) for 30 s. All the plates were continued to incubate for another 20 h or 44 h. Subsequently, 10  $\mu\text{L}$  CCK-8 solution (2 mg/mL) was added to each well and the cells were cultured for another 2 h. Then, the plates were vibrated for 8 min to obtain uniform dispersion. The absorbance value of each well at 450 nm was measured by a Thermo Scientific Microplate Reader. The untreated cells were used as blank group. The whole experiments were performed in dark. Cell viability and the half maximal

inhibitory concentration (IC50) were calculated to evaluate cells survival.

Cell viability (%)

$$= \left[ \frac{(\text{OD}_{\text{treatment}} - \text{OD}_{\text{blank}})}{(\text{OD}_{\text{control}} - \text{OD}_{\text{blank}})} \right] \times 100\%$$

### 2.10. Reactive oxygen species assay

Reactive oxygen species (ROS) in cells treated with different preparations were measured by ROS Assay Kit. Briefly, 4T1 cells were seeded on a 6-well plate at a density of  $1 \times 10^6$  cells/well and cultured for 24 h. Then, they were treated with DTX-Sol, DSD NPs, MIX-Sol, DSD/HP NPs, HP-Sol + NiR, MIX-Sol + NiR, and DSD/HP NPs + NiR, respectively. The cells treated with blank medium were used as Control group. After 4 h incubation, the cells incubated with HP-Sol + NiR, MIX-Sol + NiR, and DSD/HP NPs + NiR were additionally irradiated using a PDT laser (630 nm, 100 mW/cm<sup>2</sup>) for 30 s. All the plates were continued to incubate for another 20 h. At the scheduled time, the cells were washed with PBS once, and incubated with 1 mL of DCFH-DA (10  $\mu$ M) for 60 min. Then it was washed thrice with PBS and observed under the fluorescent microscope (DMil, Leica, Germany). The relative of DCF-fluorescence intensity was quantified.

### 2.11. Cell apoptosis assay

Apoptosis assay in each group of 4T1 cells was performed using a fluorescein isothiocyanate (FITC)-labeled Annexin V/PI assay kit. 4T1 cells were used to seed on a 6-well plate. The density of 4T1 cells and following treatment was as same as described in the section of ROS assay. After 24 h incubation, the cells were washed twice with ice-cold PBS, and then it was performed according to the manufacturer's protocol of Annexin V/PI assay kit. The percentage of apoptotic cells was analyzed by flow cytometry (BD, FACS-Calibur, USA).

### 2.12. DAPI staining assay

4T1 cells at a density of  $1 \times 10^6$  cells per well were placed on a 6-well plate and incubated for 24 h. The subsequent processing was consistent with that of ROS assay. After the cells were washed thrice with PBS, they were fixed with 4% paraformaldehyde (PFA) for 10 min. Then, 1 mL DAPI solution (1 mg/mL) was added to each well and to stain the cells for 10 min. Finally, they were washed thrice with PBS and pictured by an inverted fluorescent microscope.

### 2.13. Pharmacokinetic study

The male Sprague-Dawley (SD) rats (weight, 180–220 g) were randomly divided into 3 groups ( $n=6$ ). After fasting for 12 h, DTX-Inj, DSD NPs, and DSD/HP NPs were injected to rats via the tail vein respectively at 14.85  $\mu$ mol DTX/kg. At the pre-designated time (0.083, 0.25, 0.5, 0.75, 1, 2, 4, 6, 8, 10, 12, and 24 h), 300  $\mu$ L of blood was collected and put into a heparinized tube. After centrifugation 10 min at 13000 r/min,

plasma samples were stored at  $-80^\circ\text{C}$  until analysis. DTX concentration in blood plasma was determined by HPLC-MS/MS (Agilent 1200 (Agilent Technologies Co. Ltd.)/3200 Qtrap (Applied Biosystems, USA)). The pharmacokinetic parameters were calculated by DAS software.

#### 2.13.1. Chromatography-mass spectrometry conditions

All the samples were separated on a ZORBAX-C18 column (2.1  $\times$  50 mm, 5  $\mu$ m, Agilent, USA) at 40  $^\circ\text{C}$ . The mobile phase was consisted of methanol and water (v/v, 90:10, 0.01% trifluoroacetic acid) with a flow rate of 0.3 mL/min and injection volume of 10  $\mu$ L. The detection was carried out on an electrospray ionization source operating in positive ion mode with the multiple reaction monitoring mode. The ion transitions were 830.1 m/z  $\rightarrow$  304.2 m/z for DTX and 854.2 m/z  $\rightarrow$  309.1 m/z for PTX (internal standard), respectively. The MS parameters of desolvation temperature, curtain gas, gas 1, and gas 2 was 350  $^\circ\text{C}$ , 10 psi, 35 psi, and 20 psi, respectively.

#### 2.14. In vivo anticancer efficacy of docetaxel prodrug/hematoporphyrin co-assembled nanoparticles

100  $\mu$ L of 4T1 cells at a density of  $5 \times 10^6$  cells/mL was injected subcutaneously into the fourth pair of mammary glands of female Bal b/c mice. When tumors of mice grew to approximately 100–150 mm<sup>3</sup>, mice were randomly divided into Saline group, DTX-Inj group (12.38  $\mu$ mol DTX/kg), HP-Sol + NiR group (3.34  $\mu$ mol HP/kg), DSD-NPs group (12.38  $\mu$ mol DTX/kg), MIX-Sol + NiR group (12.38  $\mu$ mol DTX/kg), DSD/HP NPs group (12.38  $\mu$ mol DTX/kg), DSD/HP NPs-10 + NiR group (12.38  $\mu$ mol DTX/kg), DSD/HP NPs-5 + NiR group (6.19  $\mu$ mol DTX/kg), and DSD/HP NPs-3 + NiR group (3.71  $\mu$ mol DTX/kg) ( $n=6$ ). The treatments were performed every other day for five times. At 24 h post-injection, tumors of mice treated with NiR were placed in the center of light cone and irradiated with a PDT laser (630 nm, 400 mW/cm<sup>2</sup>) for 500 s (Ren et al., 2014). Tumor volume of each mouse was measured and recorded every other day, and they were calculated through the formula (width of tumor<sup>2</sup>  $\times$  length of tumor)/2. At the end of the experiment, mice were sacrificed, and hearts, livers, spleens, lungs, kidneys, and tumors were harvested for histopathological examination by hematoxylin-eosin staining (H&E) assay.

#### 2.15. Statistical analysis

Statistical significance differences between groups were evaluated using the t-test, which was calculated by SPSS 17.0.  $p < 0.05$  was considered as significant difference between the groups. All data were presented as mean  $\pm$  standard deviation (SD).

## 3. Results and discussion

### 3.1. Preparation of docetaxel prodrug/hematoporphyrin co-assembled nanoparticles

Nano-precipitation method was selected to prepare DSD/HP NPs (Li et al., 2020). Under a certain stirring speed, drugs in

absolute ethanol solution could be instantaneously self-assembled into uniform nanoparticles in water. The preparative technique of DSD/HP NPs was simple, easy, and reproducible. These self-assembled nanoparticles could be formed for several reasons. Firstly, the solubility of DTX, Do, and HP in water was poor. Secondly, both hydrophobic drugs were used to synthesize DTX-S-Do (DSD) with mono sulfide bond as a linker. So, the obtained DSD had higher lipid solubility. Thirdly, the solubility difference of DSD and HP in absolute ethanol and water was increased significantly. Because of the huge difference in solubility of drugs in absolute ethanol and water, nano-precipitation method could be used to prepare self-assembled DSD/HP NPs. And many studies had showed that hydrophobic drugs could be self-assembled into nanoparticles (Sun et al., 2018; Ma et al., 2022; Rapozzi et al., 2022; Ren et al., 2022).

### 3.2. Optimization of docetaxel prodrug/hematoporphyrin co-assembled nanoparticles

The concentration of DSD ( $X_1$ ), molar ratio of HP to DSD ( $X_2$ ), and content of stabilizer ( $X_3$ ) were selected as investigated factors. The particle size ( $Y_1$ ), PDI ( $Y_2$ ),  $EE_1$  of DSD ( $Y_3$ ), and  $EE_2$  of HP ( $Y_4$ ) were used as response values. According to the BBD, the experimental conditions were optimized using above-mentioned three factors and four levels (Table 1). All the experimental data were analyzed by the Design Expert 8.0 software with quadratic polynomial regression model equation (Tables S1–S4). The regression equations of  $Y_1$ ,  $Y_2$ ,  $Y_3$ , and  $Y_4$  were as following.

$$Y_1 = 123.48 + 38.24X_1 - 268.47X_2 - 0.85X_3 + 23.83X_1X_2 - 0.47X_1X_3 - 3.45X_2X_3 - 4.79X_1^2 + 209.00X_2^2 + 0.11X_3^2 \quad (R^2 = 0.8864, p < 0.05)$$

$$Y_2 = 0.771 - 0.232X_1 - 0.902X_2 - 0.101X_3 - 0.191X_1X_2 + 2.167E - 004X_1X_3 + 9.875E - 003X_2X_3 + 0.049X_1^2 + 1.314X_2^2 + 1.308E - 004X_3^2 \quad (R^2 = 0.9182, p < 0.05)$$

$$Y_3 = 12.87 + 20.74X_1 + 279.85X_2 + 1.53X_3 - 73.68X_1X_2 - 0.59X_1X_3 - 0.34X_2X_3 - 234.24X_2^2 - 0.02X_3^2 + 0.08X_1^2X_3 + 63.63X_1X_2^2 \quad (R^2 = 0.9550, p < 0.05)$$

$$Y_4 = 92.09 - 1.67X_1 + 0.93X_2 - 0.23X_3 + 0.86X_1X_2 - 0.15X_1X_3 - 5.00E - 003X_2X_3 + 3.23X_1^2 + 0.50X_2^2 - 1.69X_3^2 - 3.78X_1X_3^2 - 0.56X_2^2X_3 \quad (R^2 = 0.9916, p < 0.05)$$

The determination coefficients ( $R^2$ ) of four regression equations were 0.8864, 0.9182, 0.9550, and 0.9916, respectively, which indicated that the correlated degree of predicted value was high. The adjusted coefficients of determination of regression equations were 0.7403, 0.8131, 0.8800, and 0.9732, respectively, suggesting that the fitting degree of four regression models was better and the errors of experiments were small (Tables S1–S4). So, the four regression models could be used to analyze and predict the prescription of DSD/HP NPs.

The three-dimensional effect map on particle size, PDI,  $EE_1$ , and  $EE_2$  analyzed by Design Expert 8.0 software is shown in Figure 1. The optimized prescription of DSD/HP NPs was level of 1.43 ( $X_1$ ), 0.10 ( $X_2$ ), and 60 ( $X_3$ ). That is, the concentration of DSD, molar ratio of HP to DSD, and the content of stabilizer were 2 mg/mL, 0.54, and 12.46%, respectively.

According to the optimized prescription, three batches of DSD/HP NPs were prepared, and the predicted size, PDI,  $EE_1$ , and  $EE_2$  are shown in Table 2. As shown in Table 2, the absolute deviation between predicted values of the model and the measured values was less than 10%, demonstrating that the optimized model could more accurately describe the relationship of three factors (DSD concentration, HP and DSD molar ratio, and stabilizer) on particle size, PDI,  $EE_1$ , and  $EE_2$  of DSD/HP NPs.

### 3.3. Characterization of docetaxel prodrug/hematoporphyrin co-assembled nanoparticles

The optimized DSD/HP NPs were shown in a dark red appearance (Figure 2A). Two hydrophobic drugs of HP and DSD were physically mixed, together with a stabilizer TPGS to prepare co-assembled nanoparticles. And the particle size, PDI, zeta potential,  $EE_1$ , and  $EE_2$  of DSD/HP NPs were  $105.16 \pm 1.24$  nm,  $0.168 \pm 0.15$ ,  $-15.9 \pm 0.10$  mV,  $96.27 \pm 1.03$ , and  $97.70 \pm 0.20$ , respectively (Table 2). The DL of DSD and HP of DSD/HP NPs was  $69.22 \pm 1.03\%$  and  $20.03 \pm 3.12\%$ , respectively. The DL was high and the excipient content was low, indicating that the formed DSD/HP NPs could reduce the use of excipients, and decrease the side effects caused by excipients. The particle size distribution and shape of DSD/HP NPs were analyzed using Malvern Zetasizer Nano ZS90 and TEM. Figure 2(B) and (C) shows that DSD/HP NPs exhibited a narrow size distribution and homogeneous spherical shape. The particle size of DSD/HP NPs was be useful

Table 1. Box-Behnken experiment design and response values.

No.	Factors			Size ( $Y_1$ )	PDI ( $Y_2$ )	$EE_1$ ( $Y_3$ )	$EE_2$ ( $Y_4$ )
	$X_1$	$X_2$	$X_3$				
1	2.00	0.60	10.00	91.80	0.172	96.91	99.15
2	3.50	0.80	30.00	124.00	0.190	94.25	91.31
3	3.50	0.60	20.00	118.90	0.078	92.61	92.39
4	5.00	0.60	10.00	146.00	0.165	88.88	88.57
5	5.00	0.60	30.00	126.00	0.219	85.38	87.79
6	2.00	0.60	30.00	99.80	0.213	98.96	98.99
7	3.50	0.60	20.00	122.10	0.096	91.16	91.26
8	3.50	0.80	10.00	137.90	0.144	97.94	92.91
9	5.00	0.80	20.00	132.00	0.231	98.59	95.66
10	3.50	0.60	20.00	112.60	0.119	90.17	92.55
11	3.50	0.60	20.00	111.40	0.028	91.24	92.00
12	2.00	0.80	20.00	100.10	0.331	95.66	92.27
13	3.50	0.40	10.00	132.30	0.118	88.89	90.48
14	2.00	0.40	20.00	108.80	0.118	93.92	97.70
15	3.50	0.60	20.00	113.40	0.022	95.44	92.26
16	5.00	0.40	20.00	112.10	0.247	90.65	92.65
17	3.50	0.40	30.00	146.00	0.085	82.03	88.90

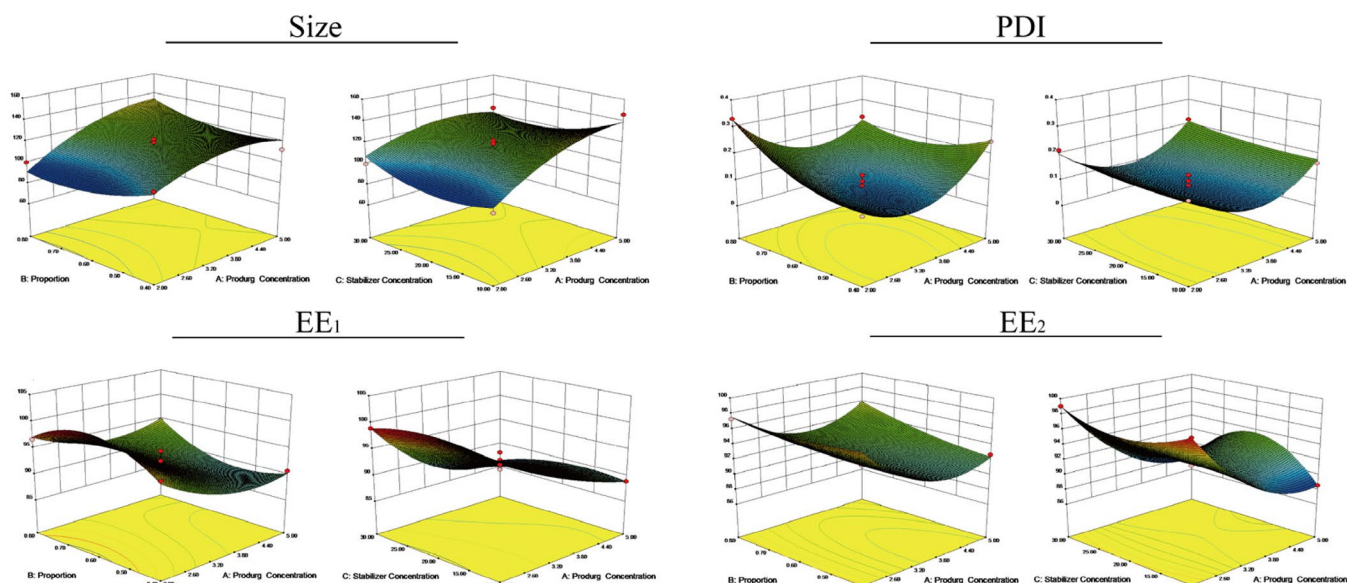


**Figure 1.** Three-dimensional effect diagram of three factors (DSD concentration, molar ratio of HP to DSD, and stabilizer) on the particle size (Size), PDI, EE of DD ( $EE_1$ ), and EE of HP ( $EE_2$ ) of DSD/HP NPs.

**Table 2.** The measured and predicted values of the optimized prescription.

Values	Experimental values	Predicted values	RE (%)
Size (nm)	105.16 ± 1.24	96.69	8.7
PDI	0.168 ± 0.15	0.155	8.4
$EE_1$ (%)	96.27 ± 1.03	98.96	-2.7
$EE_2$ (%)	97.70 ± 0.20	98.30	-0.6

for it to be accumulated passively into the tumor tissue by the enhanced permeability and retention (EPR) effect (Günay, 2020). In addition, the optimized DSD/HP NPs had negative zeta potential, which meant that DSD/HP NPs with a lower plasma protein adsorption could avoid agglomerate to some extent and was stable for the following pharmacokinetic and pharmacodynamic studies (Ivancic et al., 2020; Morales-Ol´an et al., 2021).

### 3.4. The stability of docetaxel prodrug/hematoporphyrin co-assembled nanoparticles

The physical stability and long-term stability of DSD/HP NPs in different conditions were evaluated by changes of particle size and PDI of NPs. The results are shown in Figure 2(D) and 2E. The particle size and PDI of DSD/HP NPs remained stable for 36 h in a thermostatic water bath oscillator at 37°C, and no precipitation was observed, indicating that co-assembled nanoparticles had good physical stability in water, saline, and RPMI1640 (Figure 2D). However, when it was incubated with PBS for 12 h, the particle size was increased to as 134.4 ± 1.17 nm (115.2 ± 1.76 nm for 0 h), suggesting that NPs should not be prepared and stored in PBS. After DSD/HP NPs being placed at 4°C for 30 days, there was no much difference in particle size and PDI of DSD/HP NPs in water, saline, PBS, and RPMI-1640 (Figure 2E). These results showed that the designed NPs were stable in normal human environment and cellular environment and could be used for the following *in vivo* and *in vitro* studies.

### 3.5. The release kinetics analysis of docetaxel prodrug/hematoporphyrin co-assembled nanoparticles

*In vitro* release profiles of DSD/HP NPs are presented in Figure 2(F) and (G). The cumulative release percentage of DTX released from DSD/HP NPs in PBS containing 30% ethanol and 10 mM DTT (or  $H_2O_2$ ) at 24 h was 69.3% (88.4% for  $H_2O_2$ ). These results showed that DSD/HP NPs could release DTX and HP slowly in the media of PBS with 10 mM DTT or  $H_2O_2$ , which simulated tumor redox environment and *in vivo* environment, respectively. Compared with Control group (PBS without DTT or  $H_2O_2$ ), the cumulative release percentages of drugs in release medium (PBS with DTT or  $H_2O_2$ ) were significantly different ( $p < 0.01$ ). And at the same concentration of oxidant and reductant, the released amount of DTX in oxidant condition was 1.3 times higher than that in reductant condition ( $p < 0.01$ ), indicating that DSD was more oxidizable, which in turn increased the hydrophilicity of the system and triggered the drug release (Luo et al., 2016). Furthermore, in release medium of 10 mM DTT and  $H_2O_2$ , DTX was mainly released from DSD/HP NPs in the first 12 h, while it was not released in pH 7.4 PBS only, which meant that DSD/HP NPs had good oxidation-reducing properties. In addition, the cumulative release percentage of HP released from DSD/HP NPs was found to reach 85.0% at the end of 24 h in PBS, which stimulate the extracellular environment and no appreciable release was observed from 12 h to 24 h. This co-assembled nano-drug delivery system was beneficial to prolong the stability of drug in plasma and increase the accumulation of drugs in tumor site for the subsequent *in vivo* pharmacokinetics and pharmacodynamics research.

Taken together, the prepared DSD/HP NPs was simple and stable (Figure 2G). Meanwhile, *in vitro* release data were fitted into zero order, first order, and Higuchi models to investigate the drug release mechanism, which in turn helped to formulate the prescription of DSD/HP NPs. The values of correlation coefficient (R) of each regression equation were used

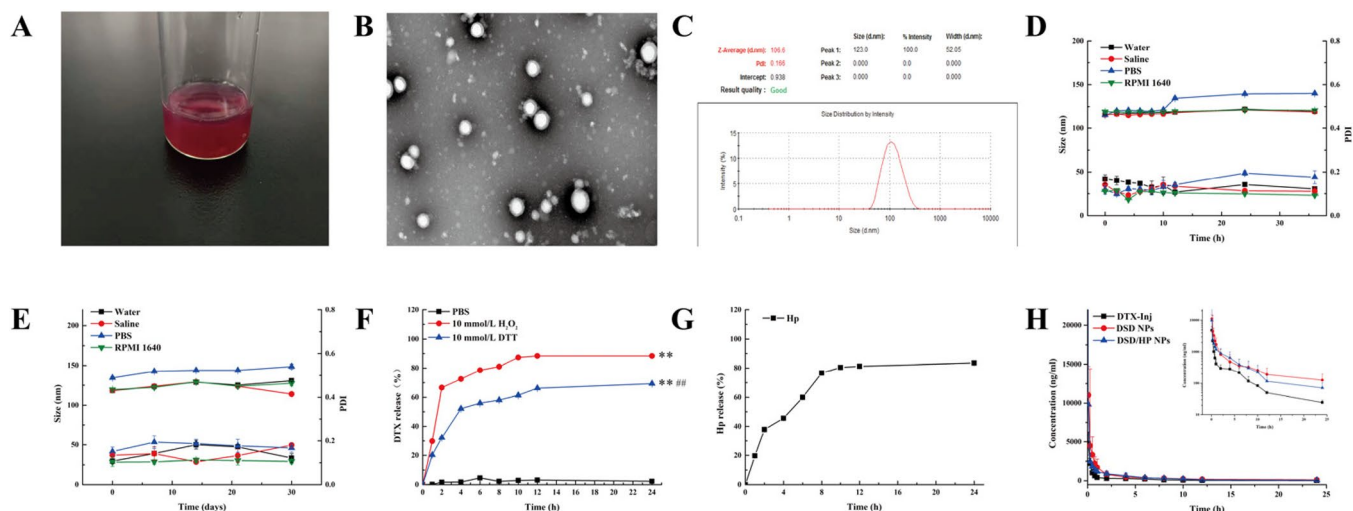


**Figure 2.** The appearance picture (A), TEM image (B), particle size distribution (C), physical stability (D), and long-term storage stability (E) of DSD/HP NPs. *In vitro* release profiles of DTX (F) and HP (G) released from DSD/HP NPs under different media. The plasma concentration time curves of DTX after intravenous injection of DTX-Inj, DSD NPs, and DSD/HP NPs at the dose of 0.01 mmol DTX/kg in rats (H) ( $n=6$ , mean  $\pm$  SD; \*\* $p < 0.01$  vs PBS group; ## $p < 0.01$  vs  $H_2O_2$  group).

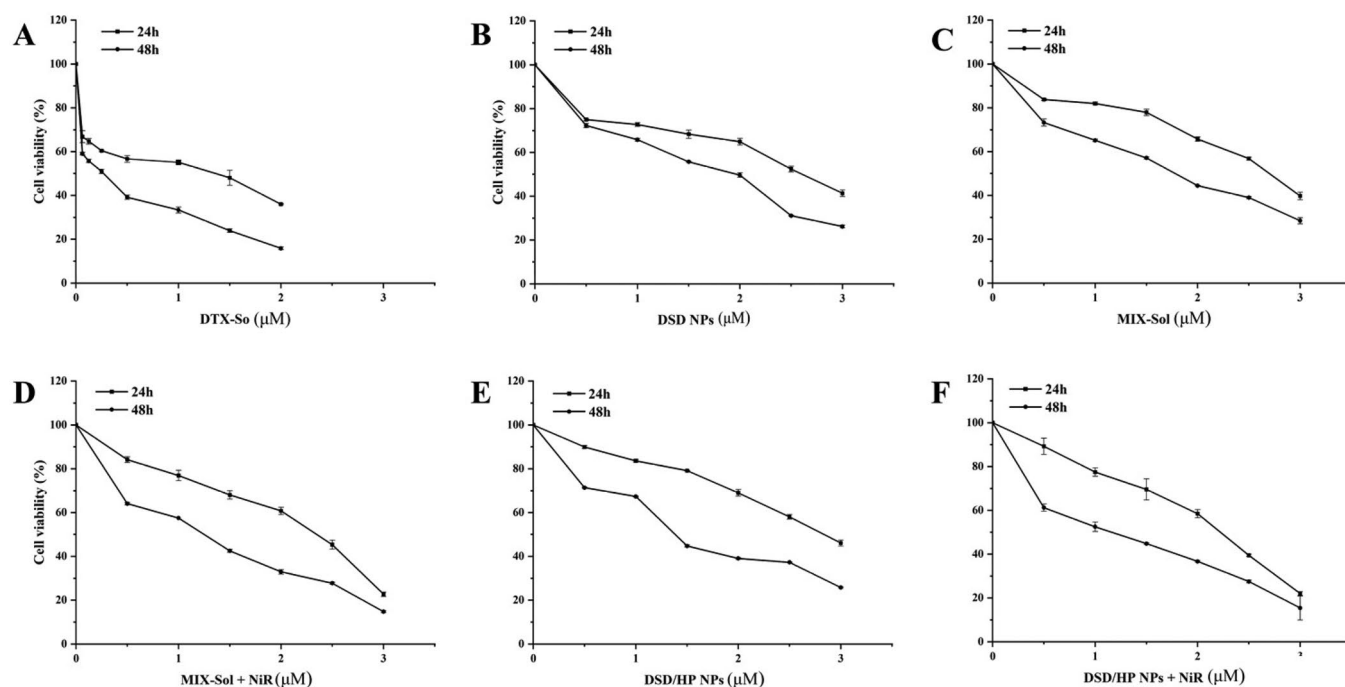


**Figure 3.** The effects of DTX-Sol (A), DSD NPs (B), MIX-Sol (C), MIX-Sol + NiR (D), DSD/HP NPs (E), and DSD/HP NPs + NiR (F) groups on cell viability in 4T1 cells after 24 h and 48 h incubation at different concentrations of DTX ( $n=3$ ).

as an evaluated index for the most suitable model (Table S5). It was observed from Table S5 that all data had good correlation with the first-order kinetics, which indicated that the release kinetics of drugs from DSD/HP NPs was best fit as the first order kinetic model.

### 3.6. Cytotoxicity analysis

The CCK-8 test showed that all groups of DTX-Sol, DSD NPs, MIX-Sol, DSD/HP NPs without the treatment of NiR, MIX-Sol + NiR, and DSD/HP NPs + NiR had good effects on the inhibition of 4T1 cell proliferation (Figure 3). And the cell viability was gradually decreased with the increase of DTX

concentration. More important, the inhibitory ability of DSD/HP NPs group under NiR was significantly stronger than that of DSD NPs group without NiR ( $p < 0.01$ ) (Figure 3E and F). The  $IC_{50}$  values of DTX-Sol, DSD NPs, MIX-Sol, DSD/HP NPs, MIX-Sol + NiR, and DSD/HP NPs + NiR at 24 h were  $0.91 \pm 0.06$ ,  $2.90 \pm 0.14$ ,  $2.73 \pm 0.12$ ,  $2.94 \pm 0.10$ ,  $2.09 \pm 0.04$ , and  $2.04 \pm 0.04 \mu M$ , respectively (Table 3). And those  $IC_{50}$  values at 48 h were  $0.19 \pm 0.01$ ,  $1.57 \pm 0.03$ ,  $1.60 \pm 0.06$ ,  $1.39 \pm 0.02$ ,  $1.03 \pm 0.07$ , and  $0.97 \pm 0.02 \mu M$ , respectively. The  $IC_{50}$  values of DSD NPs, MIX-Sol, DSD/HP NPs, MIX-Sol + NiR, and DSD/HP NPs + NiR were significantly different from that of DTX-Sol group ( $p < 0.01$ ). In addition, the  $IC_{50}$  value of DSD/HP NPs group with NiR was significantly lower than that of DSD/HP

NPs group without NiR ( $p < 0.01$ ), indicating that the introduction of PDT could obviously increase the anti-tumor effect of chemotherapy.

### 3.7. Reactive oxygen species assay

To examine changes of ROS level in response to 4T1 cells incubated with DSD/HP NPs along with or without NiR, a fluorescent microscope was used to analyze the oxidative conversion of 2'7'-dichlorofluorescein diacetate (DCFH-DA) to fluorescent DCF, and the relative fluorescence value was calculated (Figure 4). As can be seen from Figure 4(A), no obvious fluorescence was observed in 4T1 cells of Control group with or without the treatment of NiR. Among them, free drugs entered the cells quickly through passive diffusion. However, for co-assembled nanoparticles, it needed more time to enter the cells to release drugs. Therefore, ROS level generated by co-assembled nanoparticles was lower than that of DOX-Sol during the experimental time. Importantly, the data in Figure 4(B) exhibited higher ROS level of DSD/HP NPs (with NiR) compared with that of DSD/HP NPs (without NiR), suggesting that the increased ROS level of DSD/HP NPs was indeed due to the treatment of NiR ( $p < 0.01$ ). By taking advantage of different mechanisms of action of DTX and HP, synergistic anti-tumor efficacy was achieved. The design of PDT in this co-delivery nano-drug system played a positive and important role during the treatment.

### 3.8. Cell apoptosis assay and DAPI staining assay

To evaluate the apoptotic ability of DSD/HP NPs by combined PDT and chemotherapy, 4T1 cells were treated with

**Table 3.** IC<sub>50</sub> of DTX-Sol, DSD NPs, MIX-Sol, DSD/HP NPs, MIX-Sol+NiR, and DSD/HP NPs+NiR in 4T1 cells (\*\*  $p < 0.01$  vs DTX-Sol, ##  $p < 0.01$  vs DSD NPs, bb  $p < 0.01$  vs DSD/HP NPs).

Group	24 h ( $\mu\text{mol/L}$ )	48 h ( $\mu\text{mol/L}$ )
DTX-Sol	0.91 $\pm$ 0.06 ##	0.19 $\pm$ 0.01 ##
DSD NPs	2.90 $\pm$ 0.14 **	1.57 $\pm$ 0.03 **
MIX-Sol	2.73 $\pm$ 0.12 **	1.60 $\pm$ 0.06 **
DSD/HP NPs	2.94 $\pm$ 0.10 **	1.39 $\pm$ 0.02 ** ##
MIX-Sol + NiR	2.09 $\pm$ 0.04 ** ## bb	1.03 $\pm$ 0.07 ** ## bb
DSD/HP NPs + NiR	2.04 $\pm$ 0.04 ** ## bb	0.97 $\pm$ 0.02 ** ## bb

DTX-Sol, DSD NPs, HP-Sol+NiR, MIX-Sol, MIX-Sol+NiR, DSD/HP NPs, and DSD/HP NPs+NiR. The results are shown in Figure 5. Compared with Control group, DTX-Sol, DSD NPs, HP-Sol+NiR, MIX-Sol, MIX-Sol+NiR, DSD/HP NPs, and DSD/HP NPs+NiR mainly induced early apoptosis of 4T1 cells. And apoptotic characteristics of nuclear shrinkage (yellow arrow in Figure 5C) were observed in all treated groups except that in Control group. Combined the treatment of PDT and chemotherapy, nucleus shrinkage degree of 4T1 cells was strengthened, and the number of apoptotic cells was significantly increased. The percentage of apoptotic cells of DSD/HP NPs+NiR was 1.6 times higher than that of DSD/HP NPs without NiR. It could be shown that the combination of photodynamic therapy with chemotherapy designed by our research had a strong inhibitory effect on the proliferation of 4T1 cells and was beneficial to the improvement of anti-tumor efficacy.

### 3.9. Pharmacokinetic study

DTX-Inj, DSD NPs, and DSD/HP NPs were injected into the rats via tail vein, and the profiles of the mean plasma concentration of DTX versus time are illustrated in Figure 2(H). From Figure 2(H), we knew that the plasma concentration of DTX in DSD NPs and DSD/HP NPs was significantly higher than that of DTX-Inj in Control group. The main pharmacokinetic parameters of different preparations are listed in Table 4. The AUC<sub>0-t</sub> of DTX in DSD NPs and DSD/HP NPs in rats was 2.4 and 1.9 times of DTX-Inj, and the AUC<sub>0-∞</sub> was 2.7 and 2.0 times of DTX-Inj, respectively. Compared with the AUC of DTX in DTX-Inj, the AUC of DTX in DSD NPs and DSD/HP NPs was significantly increased ( $p < 0.05$ ), which could prolong DTX circulated time in blood. The results showed that DSD NPs and DSD/HP NPs were beneficial to realize the accumulation of drugs in tumor site, and increase the passive targeting of drugs to tumor. The  $t_{1/2z}$  of DTX in DSD NPs (11.01  $\pm$  5.91 h) and DSD/HP NPs (8.79  $\pm$  5.76 h) was extended in comparison with that of DTX-Inj (5.18  $\pm$  3.53 h). Although the  $t_{1/2z}$  of DTX in DSD/HP NPs group was extended to a certain extent, there was no statistical difference between DSD/HP NPs group and DTX-Inj group. The reason might be attributed to that the release of HP could produce a certain ROS in the body, which accelerated the oxidation reaction of DSD, leading to early release of DTX.

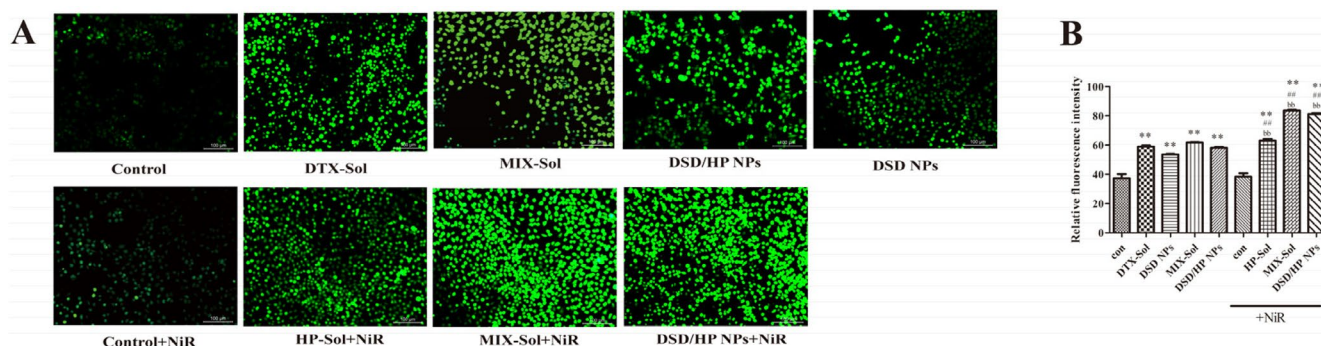


**Figure 4.** The ROS fluorescence images (A) and relative fluorescence values (B) of Control, Control+NiR, DTX-Sol, DSD NPs, HP-Sol+NiR, MIX-Sol, MIX-Sol+NiR, DSD/HP NPs, and DSD/HP NPs+NiR groups in 4T1 cells (\*\*  $p < 0.01$  vs Control group, ##  $p < 0.01$  vs DTX-Sol group, bb  $p < 0.01$  vs DSD/HP NPs group,  $n = 3$ ).



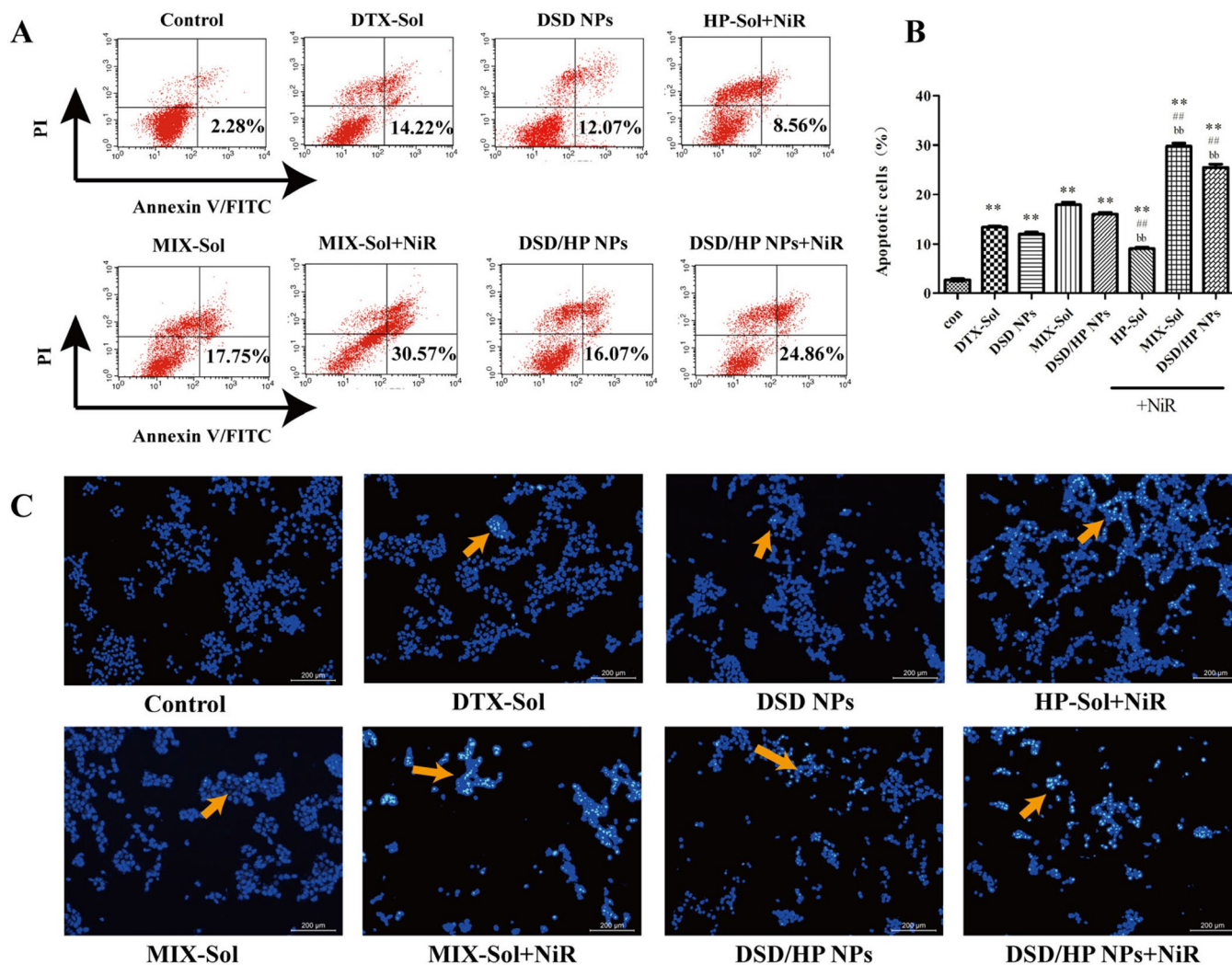


**Figure 5.** The effects of Control, Control + NiR, DTX-Sol, DSD NPs, HP-Sol + NiR, MIX-Sol, MIX-Sol + NiR, DSD/HP NPs, and DSD/HP NPs + NiR groups on 4T1 cells apoptosis. The quantitative result of Annexin V-FITC/PI double staining apoptosis assays by flow cytometry (A and B). The qualitative analysis result of DAPI staining (C) (\*\*  $p < 0.01$  vs Control group, ##  $p < 0.01$  vs DTX-Sol group, bb  $p < 0.01$  vs DSD/HP NPs group,  $n = 3$ ).

**Table 4.** Pharmacokinetic parameters of DTX in rats after treated with DTX-Inj, DSD NPs, and DSD/HP NPs ( $n = 6$ , ##  $p < 0.01$  vs DTX-Inj, #  $p < 0.05$  vs DTX-Inj).

Parameters	DTX-Inj	DSD NPs	DSD/HP NPs
AUC <sub>0-1</sub> (ng/L·h)	4724.72 ± 1139.27	11325.31 ± 5028.63 #	9016.94 ± 3588.59 #
AUC <sub>0-∞</sub> (ng/L·h)	4876.45 ± 1104.82	13351.75 ± 6118.42 ##	9817.28 ± 3612.52 #
CL <sub>z</sub> (L/h/kg)	2.55 ± 0.54	1.60 ± 1.00	1.88 ± 0.67
t <sub>1/2z</sub> (h)	5.18 ± 3.53	11.01 ± 5.91	8.79 ± 5.76
V <sub>z</sub> (L/kg)	19.32 ± 15.69	21.38 ± 8.85	26.58 ± 26.48
MRT (h)	4.018 ± 0.62	4.45 ± 1.39	4.47 ± 1.15

### 3.10. *In vivo* anticancer efficacy of docetaxel prodrug/hematoporphyrin co-assembled nanoparticles

*In vivo* antitumor efficacy of various preparations was performed in 4T1 tumor-bearing female Bal b/c mice (Figure 6). The systemic toxicity of different preparations was assessed by changes of body weights of mice (Figure 6A). The body weight of DSD/HP NPs + NiR group did not change much, suggesting that this co-assembled nano-drug delivery system had lower toxicity and good biocompatibility. Figure 6(B) shows changes of tumor volumes of mice treated with different preparations. At the end of the experiment, tumor

volumes of Saline, DTX-Inj, HP-Sol + NiR, DSD-NPs, MIX-Sol + NiR, DSD/HP NPs, DSD/HP NPs-10 + NiR, DSD/HP NPs-5 + NiR, and DSD/HP NPs-3 + NiR groups were 1240 ± 52, 611 ± 53, 688 ± 57, 566 ± 14, 680 ± 55, 535 ± 48, 395 ± 63, 491 ± 25, and 565 ± 44 mm<sup>3</sup>, respectively. The tumor volume of Saline group was the largest, and the rate of tumor growth was the fastest. Compared with DTX-Inj group, the increased tumor volume of MIX-Sol + NiR might be attributed to that MIX-Sol prepared by DTX prodrug and HP solution took a certain time for DTX prodrug to release DTX to play its anti-tumor effect. Furthermore, tumor volumes of DSD NPs, DSD/HP NPs, DSD/HP NPs-10 + NiR, DSD/HP NPs-5 + NiR, and DSD/HP NPs-3 + NiR groups were smaller than that of DTX-Inj group. The reason might be that co-assembled nanoparticles could increase the targeted accumulation of drugs in tumor site to a certain extent, and improve the anti-tumor activity *in vivo*. What was noteworthy was that DSD/HP NPs-10 with the treatment of NiR could significantly inhibit tumor growth in comparison with those who treated with DSD/HP NPs without the treatment of NiR ( $p < 0.01$ ). This result indicated that the collaborative treatment of PDT and chemotherapy had a meaningful tumor suppressive effect at the dose of 12.38 μmol DTX/kg.

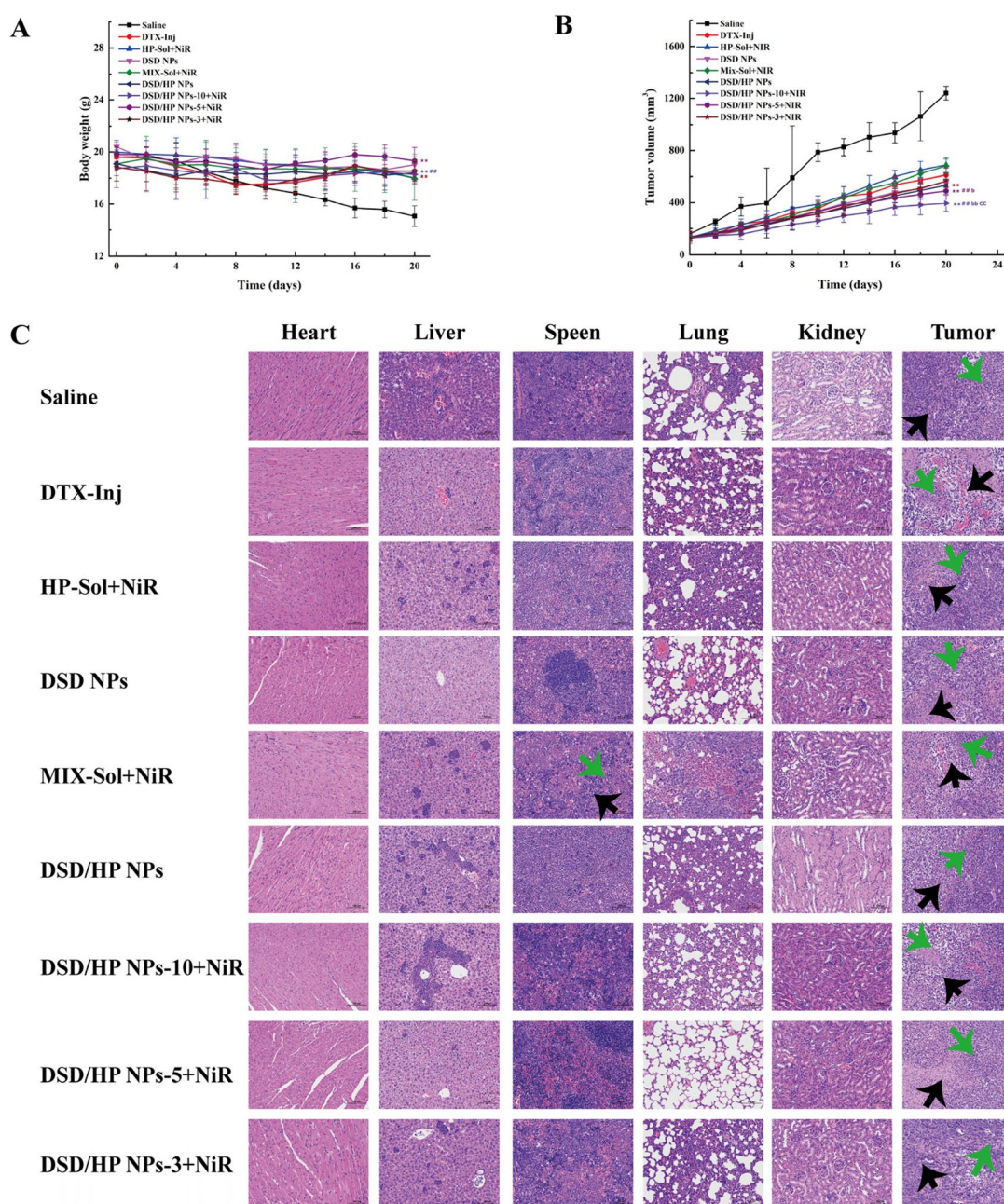


**Figure 6.** The changes of body weight (A), tumor volume (B), and H&E staining image (C) of tissues of 4T1 tumor-bearing mice treated with Saline, DTX-Inj, HP-Sol+NiR, DSD NPs, MIX-Sol+NiR, DSD/HP NPs, DSD/HP NPs-10+NiR, DSD/HP NPs-5+NiR, and DSD/HP NPs-3+NiR (\*\*  $p < 0.01$  vs Saline, ##  $p < 0.01$  vs DTX-Inj,  $b p < 0.05$ ,  $bb p < 0.01$  vs DSD NPs,  $cc p < 0.01$  vs DSD/HP NPs).

After the experiment, the main tissues of mice were collected for the analysis of H&E staining to further evaluate toxicity and antitumor effects. The result is shown in Figure 6(C). As can be seen from Figure 6(C), the clusters of tumor cells with large nuclei, atypia, and high nucleo-cytoplasmic ratio were found in tissue sections of spleen, lung, and kidney of mice in Saline group. Similarly, these characteristics were also seen locally in tissue sections of spleen and lung of MIX-Sol+NiR group (green arrow). The cortex and medulla of tissue sections of mice in DSD/HP NPs-10+NiR, DSD/HP NPs-5+NiR, and DSD/HP NPs-3+NiR groups were clearly demarcated, and glomerular capillaries were clear and no obvious structural changes were observed. The results indicated that the prepared DSD/HP NPs had no

obvious renal toxicity, and its safety was better. Compared with tumor sections of Saline group, large areas of necrotic tumor cells and hyperchromatism or fragmentation of the nucleus were observed in tumor section of DSD/HP NPs-10+NiR group (black arrow). These results illustrated that the designed co-assembled nano-drug delivery system for the combination of PDT and chemotherapy had little toxicity to normal tissues and could achieve better anti-tumor effects.

#### 4. Conclusions

In this study, DTX Prodrug and HP were successfully prepared to be as co-assembled nanoparticles. The prepared DSD/HP NPs had small particle size, high EE and DL, round

appearance, spherical shape, and good stability. It could release DTX and HP slowly in the media of pH 7.4 PBS with or without 10 mM DTT (H<sub>2</sub>O<sub>2</sub>). DSD/HP NPs along with the treatment of NiR had a better ability to inhibit 4T1 cells proliferation, and significantly induced 4T1 cells apoptosis, and produced more ROS in 4T1 cells. It also could increase and prolong the blood circulation time of DTX in rats. The most important was that DSD/HP NPs along with the treatment of NiR had obvious *in vivo* anti-tumor activity, significantly inhibited tumor growth, and low toxicity to normal tissues. As a result, DSD/HP NPs contained DTX prodrug and photosensitizer was useful for the treatment of anti-tumor. This co-assembled strategy designed in our study effectively combined nanotechnology, chemotherapy, and photodynamic therapy to provide a new idea and prospect for future comprehensive cancer treatment.

### Authors' contributions

Guolian Ren contributed to experimental design, conceptualization, funding acquisition, supervision, manuscript writing, and editing. Yujie Li contributed to experimental design and performed the experiments, figures, and tables. Canqi Ping contributed to the data analysis. Danyu Duan and Ning Li contributed to the evaluation of the preparation. Jiaqi Tang contributed to the synthesis of raw materials. Rongrong Wang and Wenju Guo contributed to the cytotoxic experiments. Xiaomin Niu and Qiuyue Ji contributed to draw the schematic illustration. Guoshun Zhang and Ruili Wang contributed to the animal studies. Shuqiu Zhang contributed to conceive the idea, funding acquisition, manuscript writing, and editing.

### Ethical approval

All animal studies were carried according to the guidelines of the Ethical Committee of Shanxi Medical University (Ethical approval number: 2019LL238).

### Data availability statement

The data used in this study to support the findings will be available from the corresponding author upon personal request.

### Disclosure statement

No potential conflict of interest was reported by the authors.

### Funding

This work was funded by the National Natural Science Foundation of China (grant number 82173767), the Research Project Supported by Shanxi Scholarship Council of China (2021-089), the Applied Basic Research Project of Shanxi Province (grant number 20210302123310), the Teaching reform of Innovation Project of Higher School of Shanxi Province (grant number J20220378), and the Science and Technology Innovation projects of Shanxi Platform Base and Talent Special Project (grant number 201805D211002).

### ORCID

Guolian Ren  <http://orcid.org/0000-0001-5468-9374>

### References

- Abrahamse H, Hamblin MR. (2016). New photosensitizers for photodynamic therapy. *Biochem J* 473:347–64.
- Agostinis P, Berg K, Cengel KA, et al. (2011). Photodynamic therapy of cancer: an update. *CA Cancer J Clin* 61:250–81.
- Allison RR, Ferguson JS. (2022). Photodynamic therapy to a primary cancer of the peripheral lung: case report. *Photodiagnosis Photodyn Ther* 39:103001.
- Castano AP, Demidova TN, Hamblin MR. (2005). Mechanisms in photodynamic therapy: part three – photosensitizer pharmacokinetics, bio-distribution, tumor localization and modes of tumor destruction. *Photodiagn Photodyn* 2:91–106.
- Chaffer CL, Weinberg RA. (2011). A perspective on cancer cell metastasis. *Science* 331:1559–64.
- Chang J-E, Yoon I-S, Sun P-L, et al. (2014). Anticancer efficacy of photodynamic therapy with hematoporphyrin-modified, doxorubicin-loaded nanoparticles in liver cancer. *J Photoch Photobio B* 140:49–56.
- Dąbrowski JM, Arnaut LG. (2015). Photodynamic therapy (PDT) of cancer: from local to systemic treatment. *Photochem Photobiol Sci* 14:1765–80.
- Fan W, Lu N, Xu C, et al. (2017). Enhanced afterglow performance of persistent luminescence implants for efficient repeatable photodynamic therapy. *ACS Nano* 11:5864–72.
- Fan W, Shen B, Bu W, et al. (2014). A smart upconversion-based mesoporous silica nanotheranostic system for synergetic chemo-/radio-/photodynamic therapy and simultaneous MR/UCL imaging. *Biomaterials* 35:8992–9002.
- Gong F, Wang R, Zhu Z, et al. (2020). Drug-interactive mPEG-b-PLA-Phe(Boc) micelles enhance the tolerance and anti-tumor efficacy of docetaxel. *Drug Deliv* 27:238–47.
- Günay MS. (2020). The formulation of methylene blue encapsulated, Tc-99m labeled multifunctional liposomes for sentinel lymph node imaging and therapy. *Turk J Med Sci* 17:381–7.
- Ivancic T, Thompson MR, Pawlak JL, et al. (2020). Influence of anionic and non-ionic surfactants on nanoparticle synthesis by solvent-free extrusion emulsification. *Colloid Surface A* 587:124328.
- Kim Y, Uthaman S, Pillarisetti S, et al. (2020). Bioactivatable reactive oxygen species-sensitive nanoparticulate system for chemo-photodynamic therapy. *Acta Biomater* 108:273–84.
- Koual M, Tomkiewicz C, Cano-Sancho G, et al. (2020). Environmental chemicals, breast cancer progression and drug resistance. *Environ Health-Glob* 19:117.
- Li C, Wang P, Wang D, et al. (2022). Fluorescence kinetics study of twice laser irradiation based HpD-PDT for nonmelanoma skin cancer. *Lasers Surg Med* 54:945–54.
- Li L, Zuo S, Dong F, et al. (2021). Small changes in the length of diselenide bond-containing linkages exert great influences on the antitumor activity of docetaxel homodimeric prodrug nanoassemblies. *Asian J Pharm Sci* 16:337–49.
- Li N, Guo W, Li Y, et al. (2020). Construction and anti-tumor activities of disulfide-linked docetaxel-dihydroartemisinin nanoconjugates. *Colloids Surf B Biointerfaces* 191:111018.
- Lisa H. (2010). Breast cancer: challenges, controversies, breakthroughs. *Nat Rev Clin Oncol* 7:669–70.
- Luo C, Sun J, Liu D, et al. (2016). Self-assembled redox dual-responsive prodrug-nanosystem formed by single thioether-bridged paclitaxel-fatty acid conjugate for cancer chemotherapy. *Nano Lett* 16:5401–8.
- Ma K, Shi J, Pei Y, et al. (2022). A carrier-free supramolecular nanoprodrug based on lactose-functionalized dimeric camptothecin via self-assembly in water for targeted and fluorescence imaging-guided chemo-photodynamic therapy. *J Colloid Interface Sci* 609:353–63.
- Menilli L, Milani C, Reddi E, et al. (2022). Overview of nanoparticle-based approaches for the combination of photodynamic therapy (PDT) and chemotherapy at the preclinical stage. *Cancers (Basel)* 14:4462.
- Morales-Ol'an G, Luna-Suárez S, Figueroa-C'ardenas JDD, et al. (2021). Synthesis and characterization of chitosan particles loaded with an-

- tioxidants extracted from chia (*Salvia hispanica* L.) seeds. *Int J Anal Chem* 2021:5540543.
- Peng J, Xiao Y, Yang Q, et al. (2021). Intracellular aggregation of peptide-reprogrammed small molecule nanoassemblies enhances cancer chemotherapy and combinatorial immunotherapy. *Acta Pharm Sin B* 11:1069–82.
- Plekhova N, Shevchenko O, Korshunova O, et al. (2022). Development of Novel Tetrapyrrole Structure Photosensitizers for Cancer Photodynamic Therapy. *Bioengineering (Basel)* 9:82.
- Rabiei R, Ayyoubzadeh SM, Sohrabei S, et al. (2022). Prediction of breast cancer using machine learning approaches. *J Biomed Phys Eng* 12:297–308.
- Rapozzi V, Moret F, Menilli L, et al. (2022). HSA-binding prodrugs-based nanoparticles endowed with chemo and photo-toxicity against breast cancer. *Cancers (Basel)* 14:877.
- Razak SAA, Gazzali AM, Fisol FA, et al. (2021). Advances in nanocarriers for effective delivery of docetaxel in the treatment of lung cancer: an overview. *Cancers* 13:400.
- Ren G, Duan D, Wang G, et al. (2022). Construction of reduction-sensitive heterodimer prodrugs of doxorubicin and dihydroartemisinin self-assembled nanoparticles with antitumor activity. *Colloid Surface B* 217:112614.
- Ren G, Jiang M, Xue P, et al. (2016). A unique highly hydrophobic anti-cancer prodrug self-assembled nanomedicine for cancer therapy. *Nanomedicine* 12:2273–82.
- Ren Y, Wang R, Liu Y, et al. (2014). A hematoporphyrin-based delivery system for drug resistance reversal and tumor ablation. *Biomaterials* 35:2462–70.
- Sun B, Luo C, Yu H, et al. (2018). Disulfide bond-driven oxidation- and reduction-responsive prodrug nanoassemblies for cancer therapy. *Nano Lett* 18:3643–50.
- Tang J, Ren G, Duan S, et al. (2020). Design and antitumor activity evaluation of n-dodecanol modified docetaxel prodrug nanostructured lipid carrier. *Chin Pharm J* 55:116–27.
- Tohkayomatee R, Reabroi S, Tungmunnithum D, et al. (2022). Andrographolide exhibits anticancer activity against breast cancer cells (MCF-7 and MDA-MB-231 Cells) through suppressing cell proliferation and inducing cell apoptosis via inactivation of ER-alpha receptor and PI3K/AKT/mTOR signaling. *Molecules* 27:3544.
- Wang D, Li C, Zhou Z, et al. (2022). Photodynamic therapy of intravenous injection combined with intratumoral administration of photosensitizer in squamous cell carcinoma. *Photodiagnosis Photodyn Ther* 38:102857.
- Wohl AR, Michel AR, Kalscheuer S, et al. (2014). Silicate esters of paclitaxel and docetaxel: synthesis, hydrophobicity, hydrolytic stability, cytotoxicity, and prodrug potential. *J Med Chem* 57:2368–79.
- Wu Y, Ding L, Zheng C, et al. (2022). Targeted co-delivery of a photosensitizer and an antisense oligonucleotide based on an activatable hyaluronic acid nanosystem with endogenous oxygen generation for enhanced photodynamic therapy of hypoxic tumors. *Acta Biomater* 153:419–30.
- Xue Y, Bai S, Wang L, et al. (2022). A dual-responsive nanoplatform with feedback amplification improves antitumor efficacy of photodynamic therapy. *Nanoscale* 14:2758–70.
- Yang Y, Sun B, Zuo S, et al. (2020). Trisulfide bond-mediated doxorubicin dimeric prodrug nanoassemblies with high drug loading, high self-assembly stability, and high tumor selectivity. *Sci Adv* 6:eabc1725.
- Zhu F, Xu L, Li X, et al. (2021). Co-delivery of gefitinib and hematoporphyrin by aptamer-modified fluorinated dendrimer for hypoxia alleviation and enhanced synergistic chemo-photodynamic therapy of NSCLC. *Eur J Pharm Sci* 167:106004.
- Zhu R, He Q, Li Z, et al. (2022). ROS-cleavable diselenide nanomedicine for NIR-controlled drug release and on-demand synergistic chemo-photodynamic therapy. *Acta Biomater* 153:442–52.